Friction **12**(9): 2126–2138 (2024)
https://doi.org/10.1007/s40544-024-0881-8
ISSN 2223-7690
CN 10-1237/TH

RESEARCH ARTICLE

Impact of surface roughness on the coefficient of friction of polymer-on-polymer contacts for deflection pulley-rope systems in the lift industry

Ainhoa GUINEA[1], Andrea AGINAGALDE[1], Wilson TATO[1], Iñigo LLAVORI[1], Pablo GARCIA[2], Leire ARRAIAGO[2], Alaitz ZABALA[1,*]

[1] *Mechanical and Industrial Production Department, Mondragon Unibertsitatea, Mondragon 20500, Spain*

[2] *Orona EIC, Orona Ideo, Hernani 20120, Spain*

Received: 05 January 2023 / Revised: 17 May 2023 / Accepted: 03 February 2024

Abstract: The coefficient of friction (CoF) between the deflection pulley and rope in a lift strongly affects the life span of the rope. Although surface roughness is a key factor affecting the metallic pulley–rope CoF, its effect on polymeric pulleys is unknown. The present study analyses the effect of roughness and working conditions on cast polyamide 6 (PA6G) deflection pulley–thermoplastic polyurethane (TPU)-coated rope contacts. The statistical analysis revealed that the effect of surface roughness on the CoF for low-load tests was significant. The present study contributes significantly to parameter selection in deflection pulley machining to minimise friction between the pulley and rope.

Keywords: polymer-on-polymer; friction; roughness; dry sliding

1 Introduction

Tribological contacts between polymers are becoming popular in industrial applications due to their low weight, low cost, good corrosion resistance, and ease of manufacture [1]. In elevators, such contacts can be found between deflection pulleys and coated ropes. Polymeric deflection pulleys are preferred over metallic pulleys due to their better comfort and noise reduction characteristics [2], and they are used in 2:1 or higher suspension system elevators (see Fig. 1) to redirect the rope to the counterweight and cabin.

The coefficient of friction (CoF) between the deflection pulley and the rope significantly affects the life span of the rope. Low-friction contacts are preferred for avoiding premature degradation of the rope. The surface roughness of the pulley crucially affects the pulley–rope contact CoF for traction metallic pulleys [3]. However, the authors found no previous work analysing the effect of roughness on polymer–polymer tribological contacts for such applications.

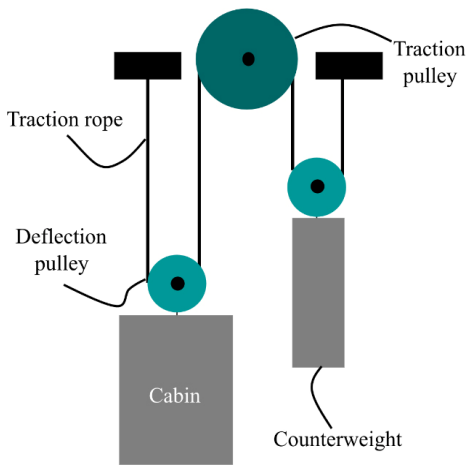

Fig. 1 Scheme of a 2:1 suspension elevator system.

Tribological contacts involving polymeric materials differ from metal–metal contact pairs. Polymers have higher adhesion forces than metallic contacts, which often results in (i) a polymeric transfer film to

* Corresponding author: Alaitz ZABALA, E-mail: azabalae@mondragon.edu

the counterpart that changes the contact pair [4, 5] and (ii) stick–slip [6]. Temperature and relative humidity significantly affect this type of contact pair. The high humidity absorption capacity of the polymers and their low heat transfer capacity lead to higher contact temperatures [1, 7], thus reducing their mechanical properties (Young's modulus [8] and shear strength [9] mainly), and directly affecting their tribological behaviour.

In contrast, the effect of contact pressure and sliding speed on the CoF in metal–polymer contacts widely varies with the study case. In 2003, Unal and Mimaroglu [10] reported that when testing polyamide 6 (PA6), polyoxymethylene (POM), and ultra-high molecular weight polyethylene (UHMWPE) against an austenitic stainless steel at a sliding speed of 0.88 m/s, the CoF increased with load. In 2004, the same author [11] tested PA66, POM, and UHMWPE against AISI D2 steel and reported that the CoF decreased when load increased a sliding speed of 1 m/s.

The effect of metal roughness on the CoF for metal–polymer tribopairs under lubricated conditions has been found to be significant. Golchin et al. [12], who tested polytetrafluoroethylene (PTFE), polyetheretherketone (PEEK), UHMWPE, and polyethylene terephthalate (PET) against Inconel 65, concluded that the effect of R_a on CoF depends on the mechanical properties of the polymer. In polymers with a high Young's modulus, the CoF decreased with increasing R_a. Niemczewska-Wójcik and Piekoszewski [13] tested UHMWPE against a titanium alloy and performed a deep 3D areal surface topography analysis of the titanium plate. They concluded that the highest autocorrelation length and texture aspect ratio, combined with the lowest root mean square slope, yielded the best tribological behaviour.

Studies on metal–polymer contacts under dry testing conditions have revealed the importance of metal surface roughness, although its effect depends on the test conditions. Kaltzakorta et al. [3] studied cast iron–thermoplastic polyurethane (TPU) tribopairs, reporting a 17% CoF decrease when increasing cast iron R_a under ambient conditions. Similarly, Harsha et al. [14] reported that an increase in titanium R_a leads to a decrease in CoF of up to 45% when rubbing against UHMWPE and cross-linked polyethylene (XLPE) under ambient conditions. Both studies associated the CoF decrease with a reduction in adhesion force due to the formation of roll-shaped wear debris in the interface. Conversely, Hausberger et al. [15] concluded that the minimum CoF is achieved either with a polished or rough surface, depending on the test conditions.

The effect of the sliding direction on the wear rate has also been reported for metal–polymer contacts. Recent studies [16, 17] analysing groove texturised 304 steel plate against a 5 wt% α-Al_2O_3 PTFE nanocomposite pin under dry conditions concluded that the perpendicular direction reduced the wear rate. The grooves acted as a wear particle trap that facilitated the formation of the transfer film and a reduction in wear. For the parallel direction, the wear particles were ejected, preventing the proper formation of the transfer film. Watanabe et al. [18] observed the opposite effect when analysing a groove texturised steel plate against a polymethyl methacrylate (PMMA) pin under lubricated conditions. When the grooves were parallel to the sliding direction, they acted as lubricant paths, thus reducing the wear. For grooves perpendicular to the sliding direction, the edges of the grooves were the starting point for exfoliation, which increased the wear rate.

Regarding polymer–polymer contacts, contact pressure and speed have a significant effect on the tribological behaviour, but there is no consensus on the effect on CoF. Unal and Findik [19] tested PA 46+30% glass fibre reinforcement (GFR) and PA 66 against polyphenylene sulfide (PPS) + 30% GFR and PA 46 +30% GFR under dry conditions. They found that the load had a nonlinear influence on the CoF, and the effect of the load varied with each tribopair. Similarly, Jia et al. [20] tested PTFE, PA66, and PPS tribopairs in dry conditions and reported that the effect of load and speed exhibited a nonlinear trend, which also varied with the tribopair. However, the effect of load and speed was negligible under lubricated conditions. Conversely, Camporez et al. [9], who studied polypropylene (PP) against PA6 under lubricated conditions, observed a decrease in CoF with increasing contact pressure.

The literature on the effect of surface roughness on

the CoF for polymer–polymer tribopairs is scarce. To the authors' knowledge, only one study considered R_a as a variable. Pogačnik and Kalin [7] analysed cast polyamide (PAG) against a POM contact pairs via a pin-on-disc test under 0.7 MPa contact pressure at different speeds (0.1, 0.5, and 1 m/s) and two POM surface roughness values (R_a = 0.2 and 0.65 μm) under dry conditions. At the lowest sliding speed, R_a = 0.2 μm corresponded to a slightly lower CoF than for higher R_a. Nevertheless, the CoF reduced when increasing the R_a at higher sliding speeds, which was associated with a decrease in the contact area, resulting in lower adhesion forces. The minimum CoF corresponded to a sliding speed of 0.5 m/s, at which the increase in R_a led to a 15% reduction in CoF.

The limited knowledge regarding polymer-on-polymer tribopairs is patent, and they should be investigated under realistic conditions for component development. The present study analyses cast polyamide 6 (PA6G) deflection pulley–TPU coated rope contacts tested under actual working conditions for elevators at contact pressures and speeds, considering the effect of PA6G surface topography and the sliding direction on the CoF.

2 Materials and methods

2.1 Friction test

Figure 2(a) shows an actual tribological system scheme comprising an elastomeric TPU-coated metallic rope sliding on a polyamide PA6G deviation pulley. The primary relative sliding movement conforms to the pulley groove in the circumferential running direction (see Fig. 2(b)). However, misalignment, which is known as fleet angle, can result in a tilted entrance of the rope into the pulley. In this misaligned state (see Fig. 2(c)), the rope contacts the groove's

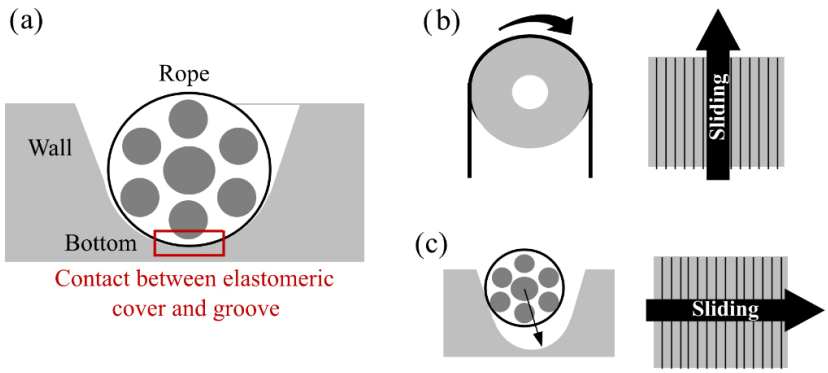

Fig. 2 (a) Real tribological contact scheme; (b) rope's sliding movement on the bottom (parallel direction); and (c) rope's sliding movement on the wall (perpendicular direction).

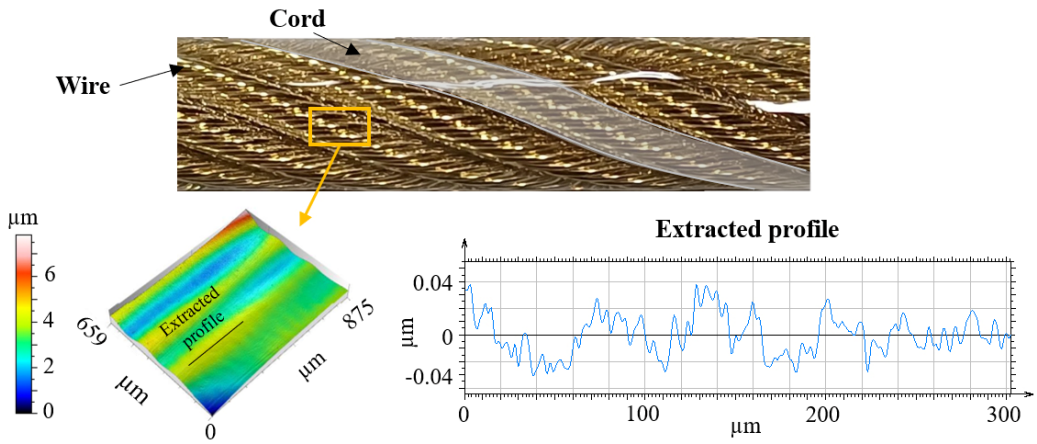

Fig. 3 Geometric and surface characteristics of the coated steel rope. Top: Top view. Bottom left: 3D surface profile. Bottom right: Extracted profile for TPU coating characterization.

wall instead of the groove bottom, causing sliding and rolling events [21]. Accordingly, two relative movements between the rope and pulley occur (parallel and perpendicular to the turning direction of the pulley).

In addition, as depicted in Fig. 3 the geometric features of both the steel cords and the individual wires constituting these cords are replicated despite the thickness of the rope coating. Consequently, the contact geometry between the pulley and the steel rope is complex.

Considering the intricate nature of the pulley-coated rope contact and relative motion, it was simplified to a reciprocating pin-on-plate test, where the rope and the pulley are simulated as the pin and plate, respectively (see Fig. 4).

Accordingly, the rolling events were not replicated and the study focused in the sliding motion. In order to approximate the complexity of the contact, the coated braided steel ropes were represented by DIN6325 steel commercial pins (ø6 mm) with a 0.5 mm-thick TPU film (which is the mean thickness of the TPU coating in actual ropes) glued at the tip using Loctite 406. It should be noted that the film roughness (R_a = 0.008 μm, R_z = 0.063 μm), resembled the roughness of the actual rope coating (R_a = 0.01 μm, R_z = 0.053 μm). PA6G plates (see material properties in Table 1) were unidirectionally milled with a 63 mm-diameter tool to obtain a surface finish similar to that of actual pulleys. Different roughness grades were generated,

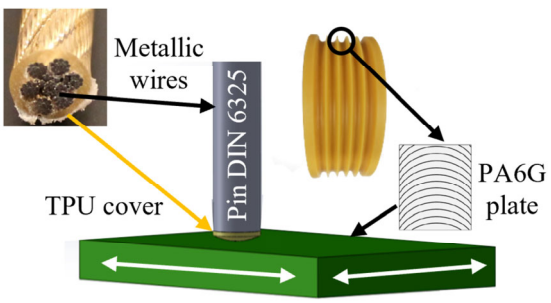

Fig. 4 Test configuration scheme.

Table 1 Material properties of the test specimens.

	PA6G plate	TPU film
Young's modulus (GPa)	3.3	0.031
Hardness (Shore D)	83	35
Glass temperature (°C)	66	-35
Poisson ratio	0.36	0.5

corresponding to R_a values of 0.2, 0.6, 2.4, and 4 μm (named *R*1, *R*2, *R*4, and *R*5, respectively). The original PA6G plate surface had an R_a of 1.2 μm with straight unidirectional marks (*R*3), which was not machined.

The real working conditions of an elevator deflection pulley–rope system were replicated in the tribological experiments. Accordingly, relative speeds of 10 and 160 mm/min and loads of 5 and 30 N were tested (which resulted in a contact pressure of 3.5 and 8 MPa, respectively). Sliding (i) perpendicular and (ii) parallel to the milling marks was tested to simulate the rope sliding against the wall and bottom of the pulley, as depicted in Figs. 2(b) and 2(c). A 9 mm stroke was selected to ensure that the milling marks could be considered straight when sliding in the parallel direction, despite being 63 mm-diameter arcs. The test duration was set to 10 cycles to allow the CoF to stabilise, and the CoF was determined through the friction energy dissipation method under the ASTM G203-10 standard, as indicated in Ref. [22]. Therefore, the CoF was calculated for each cycle as Eq. (1):

$$\mu_E = \frac{E_d}{4P\delta^*} \tag{1}$$

where P is the applied load, δ^* is the slip amplitude, and E_d is the dissipated energy over a cycle. The area enclosed by each friction envelope (the graphic representation of the friction force vs the displacement of a cycle) is the measure of E_d. Hence, E_d was obtained by performing the integral of the tangential force over the displacement interval. The final CoF value for each tested condition was the mean of the calculated μ_E for each cycle.

The pin and plate were cleaned with a lint-free WYPALL X70 cloth and alcohol before each test. The experiments were performed under controlled lab temperature (22±1°C) and relative humidity (48%±4%).

The experiments were divided into two stages to minimise the experimental effort while maintaining statistical significance. In the first stage, a full factorial design of experiment (DoE) approach was employed for a first screening of the most influential factors affecting the CoF. *R*2 and *R*4 plates were tested for all load and speed combinations in both directions. The second stage aimed to investigate the effect of surface

roughness on the CoF for the critical combinations identified in the first stage. *R*1, *R*3, and *R*5 plates were tested in the two sliding directions for the two load and speed combinations that yielded the maximum and minimum CoF in the previous stage. The test conditions for both stages are summarised in Table 2.

2.2 Surface characterisation

In-depth surface characterisations of the PAG plates were performed. PA6G plates were characterised using both 2D profile and 3D areal techniques to determine the interaction between the plate roughness and the pin.

A Mitutoyo SJ210 contact profilometer was used for profile characterisation, and R_a and R_{sm} values were computed under the EN ISO 4288 standard [23]. The *R*5 plate roughness could not be measured according to the standard due to equipment limitations in setting the required cut-off value (8 mm). Accordingly, the R_a and R_{ms} values of the *R*5 plates were computed by extracting the profile from the optical areal measurement and postprocessing it under ISO 4288 standard conditions.

A SensoFar S-NEOX optical profilometer with confocal technology [24] was used for the areal characterisation. An acquisition area of 7,892 μm × 660 μm was set to capture at least five representative motifs for PA6G plates. SensoMap Premium 7.4 metrology software was used for data postprocessing to remove the surface noise through a λs = 1.3 μm (S-filter) Gaussian filter. The form was subtracted through a second-order polynomial fitting (F-operator). Surface topography parameters belonging to height (S_a, S_q, and S_{sk}), hybrid (S_{dq} and S_{dr}), and functional (V_{mp} and V_{vv}) families were computed on the primary S-F surface as per ISO 25178 [25] for a complete description of the surfaces.

Table 2 Summary of tribological test parameters.

Pin	Commercial pin DIN6325 + TPU	
Plate	PA6G	
Lubricating medium	Dry	
Stroke (mm)	9	
Direction	Perpendicular–parallel	
Number of cycles	10	
Temperature (°C)	22±1	
Humidity (%)	48±4	
	First stage	Second stage
Load (N)	5–30	5–30
Contact pressure (MPa)	3.5–8	3.5–8
Speed (mm/min)	10–160	160
Frequency (Hz)	9.15×10^{-5} –1.48×10^{-3}	1.48×10^{-3}
Plate roughness R_a (μm)	0.6–2.4	0.2–0.6–1.2–2.4–4

2.3 Contact area determination

Due to the complexity of a tribosystem, which is composed of a hybrid metal–polymer pin against a polymeric plate (see Fig. 4), the contact area was first approximated from analytical Hertz solutions and then experimentally determined. Low-pressure Fujifilm films (2.5–10 MPa range) were used in the pin/plate interface under normal loads (5 and 30 N) to characterise the real contact area.

3 Results and discussion

3.1 Surface characterisation results

Table 3 lists all the results obtained from the 2D and 3D surface characterisation of the PA6G plates. The measured R_a values were in good agreement with the targeted R_a values. R_{sm} denotes the distance between the peaks corresponding to machining marks. Notably, the R_{sm} value of *R*5 is larger than the contact area for low load cases (see Section 3.2 Second stage results). Consequently, *R*5 should not be considered as typical surface roughness, but rather as a distinctive geometric feature. Therefore, the roughness of the areas between the peaks (referred as peak–flank area for the rest of the document) were analysed by cropping and removing the form with a plane (see Table 4). The 2D average roughness values (R_a) and 3D values (S_a) as well as the root mean square roughness (S_q) exhibited the same trends, with *R*1 being the smoothest surface and *R*5 the roughest. The skewness parameter (S_{sk}) represents the shape of the height distribution. All the surfaces except *R*3 exhibited positive skewness, indicating a predominance of peaks. This surface exhibited a negative S_{sk}, implying a predominance of valleys, which may be attributable to its different

Table 3 Surface characterisation 2D and 3D for PA6G plates. The *R*5* "peak–flank" area are the topographic parameters for the areas between the peaks of *R*5 plate.

	*R*1	*R*2	*R*3	*R*4	*R*5	*R*5* "peak–flank" area
R_a (µm)	0.179±0.014	0.467±0.019	1.202±0.025	2.535±0.025	4.045±0.156	0.280±0.029
R_{sm} (mm)	0.027±0.004	0.070±0.003	0.216±0.017	0.830±0.119	1.226±0.140	0.033±0.002
S_q (µm)	0.325±0.004	0.705±0.033	1.810±0.118	2.844±0.305	4.600±0.453	0.567±0.082
S_a (µm)	0.246±0.007	0.557±0.038	1.367±0.047	2.391±0.246	3.779±0.314	0.434±0.055
S_{sk}	0.642±0.794	0.891±0.295	-0.109±0.503	0.448±0.168	0.980±0.381	0.767±0.275
S_{tr}	0.660±0.140	0.044±0.003	0.218±0.043	0.488±0.007	0.607±0.009	0.147±0.058
S_{dq} (°)	0.175±0.018	0.212±0.018	0.180±0.013	0.280±0.063	0.490±0.141	0.136±0.002
S_{dr} (%)	1.465±0.281	1.920±0.243	1.391±0.141	2.288±0.370	3.791±0.859	0.895±0.025
V_{mp} (p = 10%) (µm^3/µm^2)	0.019±0.004	0.037±0.006	0.085±0.013	0.100±0.004	0.238±0.045	0.041±0.011
V_{vv} (p = 80%) (µm^3/µm^2)	0.040±0.007	0.058±0.003	0.248±0.075	0.162±0.011	0.242±0.023	0.053±0.007

Table 4 3D and 2D profiles of PA6G plates at imposed and free scale.

Plate	3D profile (imposed height scale)	2D profile (free height scale)	Peak-flank "Flat" areas
*R*1	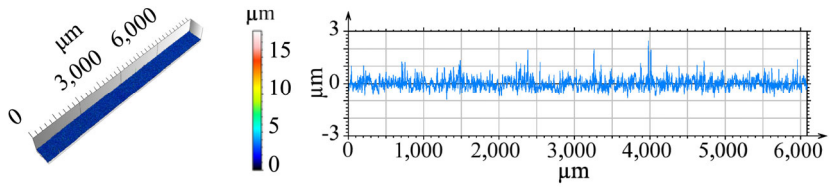		
*R*2	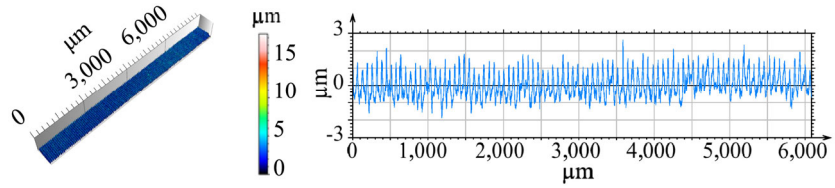		
*R*3	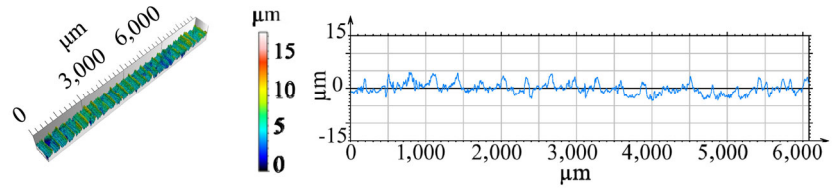		
*R*4	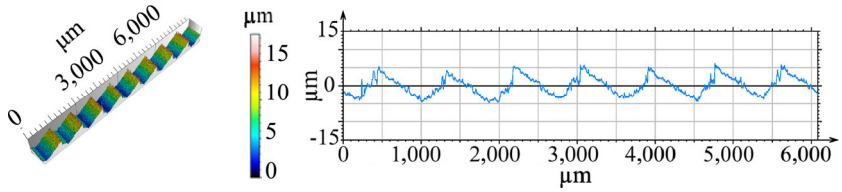		
*R*5	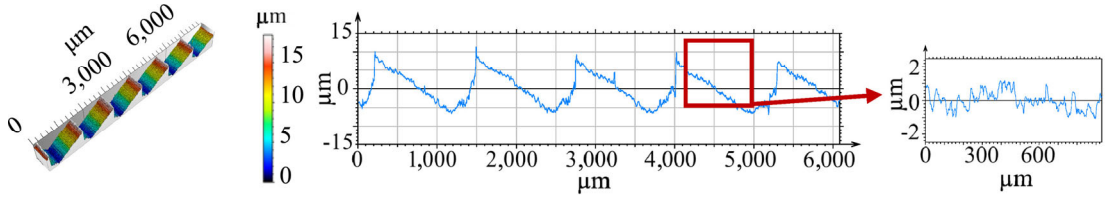		

fabrication process (the *R*3 sample was not machined). The hybrid parameter S_{dq} represents the root mean square of the surface slope. Its trend generally agreed with the height parameter values (R_a and S_a), that is, *R*1 and *R*5 had the lowest and highest values, respectively. *R*3 and peak–flank area were an exception with a lower S_{dq} value than *R*2 and *R*1, respectively. The S_{dr} describes the developed interfacial area of the surface, representing the supplementary percentage of surface area provided by its texture in comparison to an ideal planar surface. It is conformed to the same trend as the S_{dq} parameter.

V_{mp} and V_{vv} were calculated from the Abbot–Firestone curve, corresponding to the peak and void volumes and computed at 10% and 80%–100% of the material ratio, respectively. V_{mp} and V_{vv} trends agreed with the R_a and S_a values. Again, *R*3 exhibited a larger V_{vv} than *R*4.

Table 4 lists the 3D (at imposed height scale) and 2D profiles (at a free-height scale) extracted from the 3D areal measurements. In addition, it includes the 2D profile of the peak–flank area for *R*5 plate.

3.2 First stage results

Figure 5 shows the Pareto chart of the first stage of the DoE study which is used to determine the magnitude and important of the experimental variables and their interactions using a risk factor of 0.05. The risk factor signifies the probability of erroneously asserting the existence of a statistically significant effect when, in reality, it does not exist.

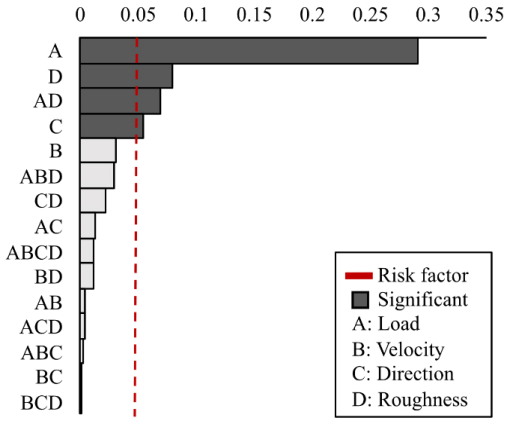

Fig. 5 Pareto diagram of the experimental first stage. The reference line is the threshold for considering a factor significant according to the 0.05 risk factor.

For this analysis, the significance level was set at 5%. Each of the test variables is denoted as a letter being load (A), velocity (B), direction (C), and roughness (D). The interaction between variables is denoted by concatenating the assigned variables letters. For instance, load–velocity interaction is represented by AB. Three of the four factors under study were statistically significant (load, roughness, and sliding direction), and the interaction between the load and roughness was significant. The impact of velocity was negligible, as expected for the studied range of velocities [26].

Figure 6 shows the effects of the statistically significant factors on the CoF as their magnitudes increase. The CoF decreases significantly when load is increased, which is expected for rigid body–elastomer contact pairs [27], corroborating previous reports on steel–TPU [28] and cast iron–TPU [29] contacts. The same behaviour was observed when testing nylon against steel [30]. Conversely, the CoF increased when the R_a value was augmented and the sliding direction and milling marks were aligned. Regarding the significant interactions, the influence of the surface roughness decreases as the load increases (see Fig. 6(d)).

Figure 7 shows all the results corresponding to the stage one analysis. As previously mentioned, the roughness is significant at low loads, and the effect is negligible at high loads.

Due to the effect of velocity being insignificant, the second stage of analysis was performed at high speed to save time. However, differences in friction loops were observed when the speed was changed. Figure 8 shows representative friction loops at high and low loads at both speeds, which exhibited different friction mechanisms. For high-load tests, both speeds exhibited a clean CoF signal, whereas for low-load tests, the low speed case exhibited a noisy signal. The test frequency of the low load–low speed signal (6.9 Hz for *R*4) did not match the plate roughness frequency (0.2 Hz for *R*4), which invalidates the notion of geometric interaction between the peaks of the pin and plate due to the R_{sm} values of the plate. Therefore, the noise at low loads was related to a stick–slip phenomenon, which is more likely to occur at low velocities in rubber materials [28].

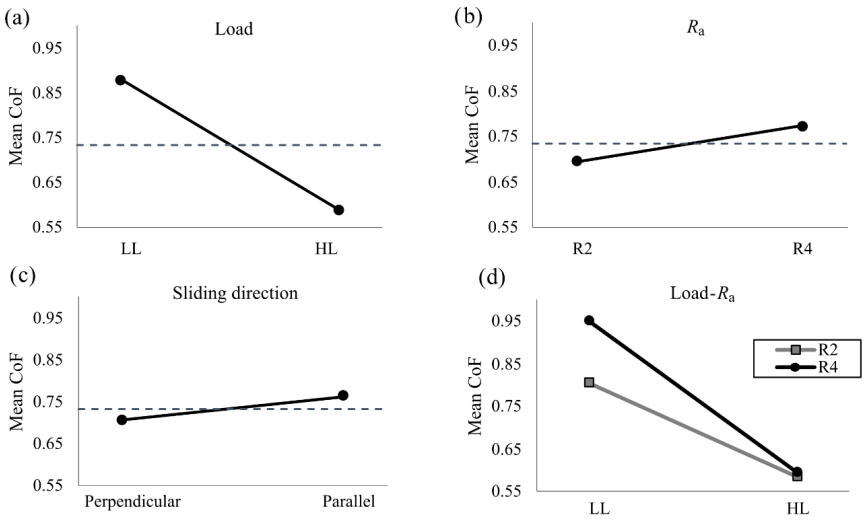

Fig. 6 Influence of statistically significant factors. (a) Load: Low load (LL) and High Load (HL); (b) R_a: *R*2 and *R*4; (c) sliding direction: perpendicular and parallel; and (d) load-R_a on the mean CoF.

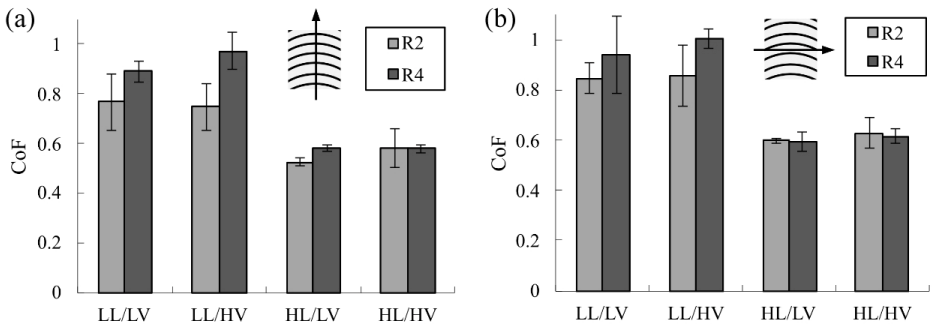

Fig. 7 CoF results for Low Load (LL), High Load (HL), Low Velocity (LV), and High Velocity (HV) combinations for *R*2 and *R*4 in (a) perpendicular direction and (b) parallel direction.

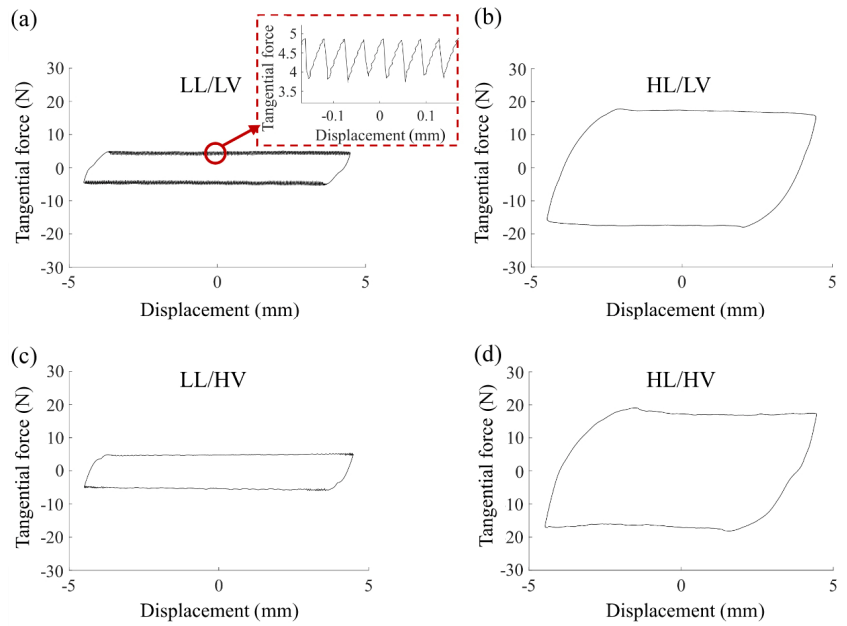

Fig. 8 *R*4 friction loops results for the perpendicular direction. (a) Low Load (LL)/Low Velocity (LV); (b) Low Load (LL)/High Velocity (HV); (c) High Load (HL)/Low Velocity (LV); and (d) High Load (HL)/High Velocity (HV).

3.3 Second-stage results

Figure 9 shows the second-stage results, at which all the roughness values under analysis (*R*1-*R*2-*R*3-*R*4-*R*5) were tested for one speed (HV) and two loads (LL, HL). At high loads, the roughness has no effect on friction in both directions (perpendicular and parallel). Conversely, at low load conditions, surface roughness has almost no effect on sliding in the parallel direction (Fig. 9(b)), but the effect is significant in the perpendicular direction (Fig. 9(a)). A nonlinear effect was observed at low load conditions in the perpendicular direction. The CoF first reduces when the roughness increases, with a minimum R_a of 0.6 μm. Afterward, the CoF increases as the roughness increases, peaking at R_a 2.4 μm. Finally, it reduces again at a surface roughness of R_a 4 μm.

Different wear mechanisms were observed on the pin TPU surfaces tested at low and high loads (see Fig. 10). Pins tested under low load exhibited smooth and homogeneous surfaces (Fig. 10(b)), which were similar to the nontested surfaces (Fig. 10(a)). Conversely, buckles or waves of detachments appeared on high-load-tested TPU pin surfaces (see Fig. 10(c)), which correspond to Schallamach waves [15, 29, 31, 32]. Schallamach waves are generated because of the small elastic limit of TPU (100 times smaller than that of PA6G) and relatively large adhesion energy [31]. The rolls generated due to this wear mechanism (see Fig. 10(d)) remain in the contact interface, acting as a solid lubricant, which explains the observed decrease in friction relative to that in the low load case. This change in tribological contact dominates the friction in high-load tests, invalidating the effect of PA6G surface roughness. These results agree with previously published data on TPU tribopairs [3], where a drop in the CoF and a decrease in the roughness effect were reported when Schallamach waves were observed.

The low-load tests reveal that the surface roughness influences the CoF. To clarify the roughness interaction, the contact area and surface motives interacting in the tribological contact were further analysed. Figure 11 shows the experimental and analytical (Hertz solution) results of the contact pressure and contact area for low- and high-load tests.

Notably, the analytical Hertz solution does not represent the complex contact system of the present study because the pin is composed of a rigid metallic bulk covered by a non-rigid TPU coating. Accordingly, experimental results differed from the analytical solutions (lower contact area and higher mean contact pressure). The experimental results revealed a contact

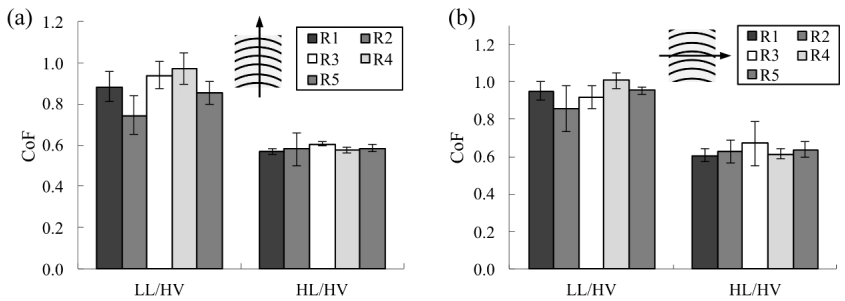

Fig. 9 Low Load/High Velocity and High Load/High Velocity CoF results for (a) perpendicular direction and (b) parallel direction.

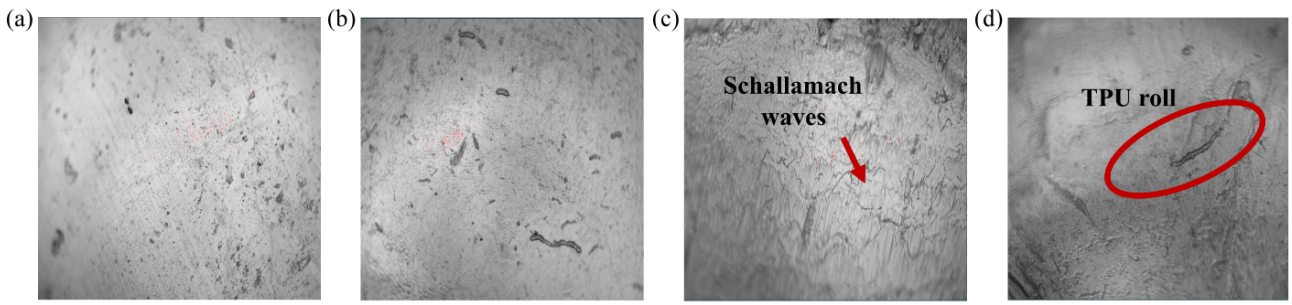

Fig. 10 Pin's TPU film surface under (a) non tested conditions; (b) LL/HV conditions for *R*4; (c) HL/HV conditions for *R*5; and (d) HL/HV for *R*4.

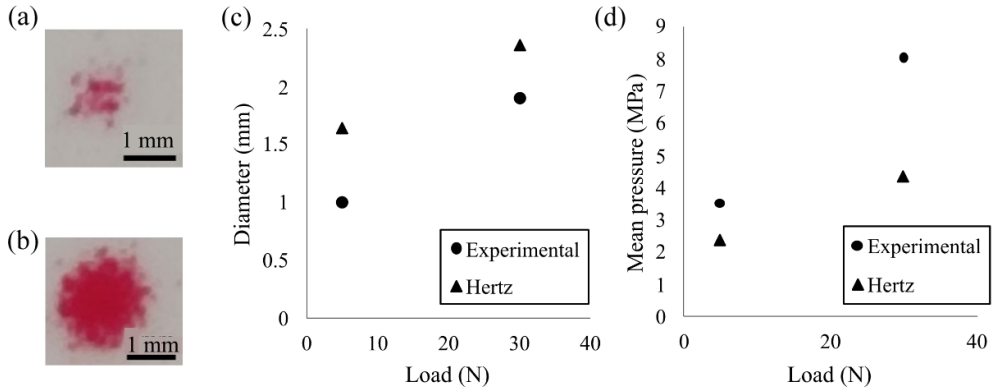

Fig. 11 Experimental test and Hertz model result comparison: (a) Fujifilm low-pressure films test results at LL conditions; (b) Fujifilm low-pressure films test results at HL conditions; (c) contact diameter; and (d) mean contact pressure.

area of 0.79 and 2.83 mm^2 and a contact pressure of 3.5 and 8 MPa for the low- and high-load cases respectively. The PA6G roughness peaks in contact with the TPU pin were determined by considering the contact area for the low-load tests (0.79 mm^2)and 2D Rms parameter (see Fig. 12(a)).

For *R*5 the distance between the peaks was larger than the dimension of the contact. As a result, the peak flank area (see Table 4) became the contact surface and its roughness assumed greater significance in the CoF behaviour (see Table 3). A schematic of the contact mode, considering the contact area and R_{sm} values of the plates, is shown in Fig. 12(b).

Considering the large differences between the contact areas in Fig. 12(b), the S_{dr} value (the developed interfacial area of the surface), in addition to R_a, has been considered for analysing the obtained CoF results. Figure 13 presents the obtained CoF results for both directions as well as the R_a and S_{dr} values of each plate. The results are presented in ascending order of the R_a plates.

Perpendicular direction tests reveal a CoF reduction when the R_a is increased until it reaches its minimum value, corresponding to the *R*2 surface (Fig. 13). However, this trend is not consistent with the S_{dr} parameter evolution. An increase in S_{dr} results in a more developed surface, which would result in a larger contact area and stronger adhesion forces (resulting in increased friction). The increase in S_{dr} value and reduction in CoF value of the *R*2 surface suggest that the TPU is incapable of adapting to all the developed areas due to the small R_{sm} value, preventing the whole contact of the TPU surface. The contact area decreases with adhesion force, resulting in a lower friction coefficient. These results corroborate previous findings. Fujita et al. [33] analysed elastomer tips against texturised glass surfaces, reporting a smaller CoF in the textured glass surfaces due to the reduction in adhesion resulting from the apparent contact area diminution.

Beyond *R*2, the CoF value increases with R_a. As the R_a value increases, the effect of adhesion may reduce,

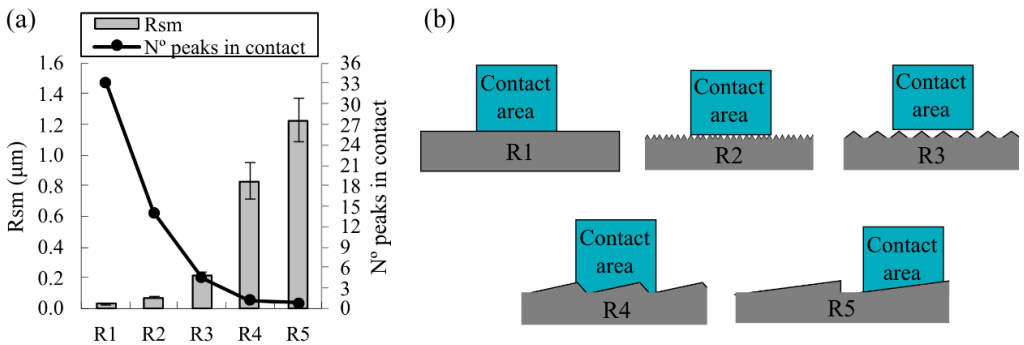

Fig. 12 Relationship between plate surface R_{sm} values and the number of peaks in contact for low load cases. (a) R_{sm} and number of peaks in contact for each roughness and (b) schematic of the contact PA6G plates considering the experimental contact area.

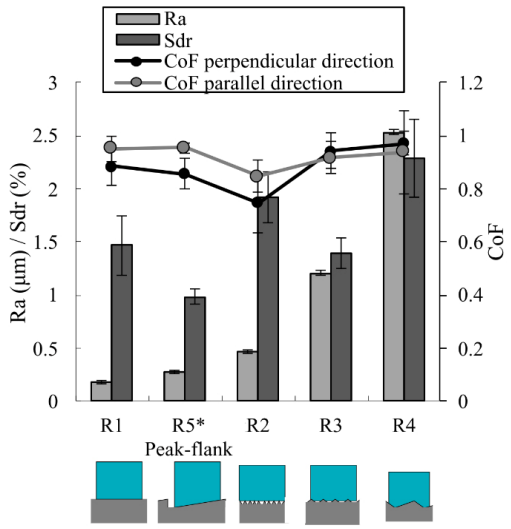

Fig. 13 Relationship between the R_a and S_{dr} values of the surfaces and the CoF. * The presented values of the *R*5 plate correspond to the peak–flank areas (see Table 4).

and the hysteresis may be the predominant effect on the CoF. Therefore, the CoF is augmented when increasing the R_a as the elastic deformation of the TPU is increased [34]. Regarding the S_{dr} values, different trends were observed. On the one hand, *R*3 exhibited a smaller S_{dr} than *R*1 and a larger CoF. Notably, the *R*3 plate was not machined and exhibited a negative S_{sk} (predominance of valleys in the surface), which may change the plate behaviour. On the other hand, *R*4 exhibited the maximum S_{dr} and R_{sm} values, which may enable the TPU to adapt to all the developed surfaces, maximising the contact area. This increases the adhesion forces and, consequently, the CoF value. Further studies are required to determine whether the increase in CoF is associated with an increase in adhesion forces or hysteresis.

Regarding the CoF results in the parallel direction, Fig. 13 reveals that the differences in the CoF between the plates are subtle. Nevertheless, the trends of the parallel and perpendicular directions are similar. In the parallel direction, hysteresis cannot be predominant as the pin does not slide against the asperities of the plates, which reinforces the idea of CoF augmentation due to an increase in the contact area. The S_{dr} value does not fully correlate with the CoF because the TPU may not be able to adapt to all the developed surfaces.

Further work is needed to clarify whether the CoF augmentation corresponding to an increase in the R_a is due to hysteresis or augmentation of the real contact area. The capacity of TPU to adapt to the surface should also be characterised to elucidate the interaction between friction and roughness.

4 Conclusions

The effect of pulley roughness and sliding direction on the coefficient of friction (CoF) of pulley–rope contacts was analysed through reciprocating tests. The statistical analysis revealed that the surface roughness and sliding direction have a significant effect on the friction coefficient during low-load tests. The following conclusions can be drawn:

1) The effect of speed on CoF is negligible for the studied ranges (10–160 mm/min). However, a stick–slip phenomenon was identified only in low-load and low-velocity cases.

2) The most influential variable on the CoF is load because it changes the friction mechanism. High contact pressure generates thermoplastic polyurethane (TPU) rolls that stay in the interface and act as solid lubricants. Therefore, the CoF decreases, and the cast polyamide 6 (PA6G) surface roughness effect becomes negligible.

3) The surface roughness only becomes relevant for low-load cases.

4) Both the S_{dr} (developed interfacial area) and R_{sm} (arithmetic mean value of the width of the roughness profile elements within the sampling length) parameters are important for elucidating the interaction between roughness and CoF. A bigger interfacial area corresponds to a higher adhesion force, leading to an increase in friction. However, depending on the R_{sm} value, the TPU might not be able to adapt to the PA6G surface, decreasing the apparent contact area and thus the CoF.

5) For large R_a values, the CoF increase may be related to (i) an increase in the hysteresis caused by the larger elastic deformation of the TPU generated by bigger asperities or (ii) a larger contact area—as with large R_{sm} values, the TPU may be able to adapt to all the developed surface.

6) The effect of surface roughness in the parallel direction is weaker than that in the perpendicular direction, but the trend is consistent.

Future work should clarify whether the CoF augmentation that occurs with increasing R_a is caused by augmentation of the real contact area or hysteresis. The present study can guide the parameter selection for deflection pulley machining to minimise friction between the pulley and rope.

Acknowledgements

This work was financially supported by the Basque Government under the "Programa de Red Guipuzcoana de Ciencia, Tecnología e Innovación" (Project ASEFI: Investigación y análisis de estrategias para incrementar la eficiencia energética del ascensor, Ref. 76187) and by ORONA EIC.

Declaration of competing interest

The authors have no competing interests to declare that are relevant to the content of this article.

References

[1] Bashandeh K, Lan P, Polycarpou A A. Tribological performance improvement of polyamide against steel using polymer coating. *Tribol Trans* **62**: 1051–1062 (2019)

[2] Bernd Nussdorfer. The Use of Nylon Pulleys in Elevators. https://elevatorworld.com/article/the-use-of-nylon-pulleys-in-elevators/, 2022.

[3] Kaltzakorta O, Wäsche R, Hartelt M, Aginagalde A, Tato W. Influence of polymer filler on tribological properties of thermoplastic polyurethane under oscillating sliding conditions against cast iron. *Tribol Lett* **48**: 209–216 (2012)

[4] Pogačnik A, Kupec A, Kalin M. Tribological properties of polyamide (PA6) in self-mated contacts and against steel as a stationary and moving body. *Wear* **378–379**: 17–26 (2017)

[5] Wang M, Zhang C, Wang X. The wear behavior of textured steel sliding against polymers. *Materials* **10**: 330 (2017)

[6] Dong C, Yuan C, Bai X, Qin H, Yan X. Investigating relationship between deformation behaviours and stick-slip phenomena of polymer material. *Wear* **376–377**: 1333–1338 (2017)

[7] Pogačnik A, Kalin M. Parameters influencing the running-in and long-term tribological behaviour of polyamide (PA) against polyacetal (POM) and steel. *Wear* **290–291**: 140–148 (2012)

[8] Ramesh V, van Kuilenburg J, Wits W W. Experimental analysis and wear prediction model for unfilled polymer–polymer sliding contacts. *Tribol Trans* **62**: 176–188 (2019)

[9] Camporez R M, Strey N F, Machado V M, Scandian C. On the reciprocating sliding wear of polypropylene against polyamide 6 in dry and aqueous environments. *Wear* **426–427**: 1018–1025 (2019)

[10] Unal H, Mimaroglu A. Friction and wear behaviour of unfilled engineering thermoplastics. *Mater Des* **24**: 183–187 (2003)

[11] Unal H, Sen U, Mimaroglu A. Dry sliding wear characteristics of some industrial polymers against steel counterface. *Tribol Int* **37**: 727–732 (2004)

[12] Golchin A, Nguyen T D, De Baets P, Glavatskih S, Prakash B. Effect of shaft roughness and pressure on friction of polymer bearings in water. *Proc Inst Mech Eng Part J J Eng Tribol* **228**: 371–381 (2014)

[13] Niemczewska-Wójcik M, Piekoszewski W. The surface texture and its influence on the tribological characteristics of a friction pair: Metal–polymer. *Arch Civ Mech Eng* **17**: 344–353 (2017)

[14] Harsha A P, Wäsche R, Joyce T J. Wear of biopolymers under reciprocating sliding conditions against different counterfaces. *Polym Eng Sci* **59**: 2356–2366 (2019)

[15] Hausberger A, Major Z, Theiler G, Gradt T. Observation of the adhesive- and deformation-contribution to the friction and wear behaviour of thermoplastic polyurethanes. *Wear* **412–413**: 14–22 (2018)

[16] Ye J, Zhang K, Gao T, Zhang Y, Liu X, Liu K. Self-competing and coupled effect of laser-engraved counterface groove depth and density on wear of alumina PTFE. *Tribol Lett* **67**: 56 (2019)

[17] Zhang K, Liu K, Gao T, Qiao Y, Zhang Y, Liu X, Wang W,

Ye J. The unrecognized importance of roughness directionality to polymer wear. *Wear* **486–487**: 204084 (2021)
[18] Watanabe S, Kodama E, Sakakibara K, Sasaki S, Tsujii Y. Effect of surface texturing on the durability of concentrated polymer brushes. *Tribol Int* **155**: 106668 (2021)
[19] Unal H, Findik F. Friction and wear behaviours of some industrial polyamides against different polymer counterparts under dry conditions. *Ind Lubr Tribol* **60**:195–200 (2008)
[20] Jia B Bin, Liu X J, Cong P H, Li T S. An investigation on the relationships between cohesive energy density and tribological properties for polymer-polymer sliding combinations. *Wear* **264**: 685–692 (2008)
[21] Nakajima M, Nakayama M, Ohnuki O, Nishino K. Elevator Device. WO2020110245A1, 2020.
[22] Llavori I, Zabala A, Aginagalde A, Tato W, Ayerdi J J, Gómez X. Critical analysis of coefficient of friction derivation methods for fretting under gross slip regime. *Tribol Int* **143**: 105988 (2020)
[23] ISO 4288:1996/COR 1:1998 Geometrical Product Specifications (GPS) — Surface texture: Profile method — Rules and procedures for the assessment of surface texture — Technical Corrigendum 1. ISO, 1996.
[24] Tato W, Blunt L, Llavori I, Aginagalde A, Townsend A, Zabala A. Surface integrity of additive manufacturing parts: A comparison between optical topography measuring techniques. *Procedia CIRP* **87**: 403–408 (2020)
[25] ISO 25178-2 2012 Geometrical product specifications (GPS)- Surface texture: Areal: II. terms, definitions and surface texture parameters. ISO, 2012.
[26] Persson B N J, Albohr O, Tartaglino U, Volokitin A I, Tosatti E. On the nature of surface roughness with application to contact mechanics, sealing, rubber friction and adhesion. *J Phys Condens Matter* **17**: R1–R62 (2005)
[27] Roger Brown. *Physical testing of rubber, 4th Ed*. New York (USA): Springer, 2006.
[28] Li C, Huang H, Qu J, Cao J, Huang F, Wang Y. Mechanism of wear and COF variation of vulcanized rubber under changing loads and sliding velocities: Interpretation at the atomic scale. *Tribol Int* **170**: 107505 (2022)
[29] Luis Angel Bartolomé. Theoretical, experimental and numerical analysis of mechanical and contact behaviours of a thermoplastic polyurethane elastomer used as cover rope in lift industry. Ph.D. Thesis. Mondragon (Spain): University of Mondragon, 2012.
[30] Nuruzzaman D M, Chowdhury M A, Rahaman M L, Oumer A N. Influence of normal loads and sliding velocities on friction properties of engineering plastics sliding against rough counterfaces. *IOP Conf Ser Mater Sci Eng* **114**: 012112 (2016)
[31] Cui Z, Su Z, Hou D, Li G, Wu J, Su B, Liu Y, Wang Y. From small wrinkles to Schallamach waves during rubber friction: In situ experiment and 3D simulation. *Polym Test* **96**: 107084 (2021)
[32] Schapery R A. A model for the prediction of rubber friction with Schallamach waves. *Tribol Int* **143**: 106018 (2020)
[33] Fujita N, Yamaguchi H, Kinoshita T, Iwao M, Nakanishi Y. Friction behaviors of elastic materials sliding on textured glass surfaces. *Tribol Int* **171**: 107539 (2022)
[34] Fuller K N G, Tabor D. The effect of surface roughness on the adhesion of elastic solids. *Proc R Soc London Ser A, Math Phys* **345**: 327–342 (1975)

Ainhoa GUINEA. She received her bachelor degree in mechanical engineering in 2021 from Mondragon University, Spain. This publication is related to the research she conducted during her degree's final project. Presently, she is a Ph.D. student at the same university, working in collaboration with two research groups, surface technologies and advanced material forming processes. Her doctoral work focuses on developing a design tool for surface textures applied to tools in sheet metal forming applications. This involves modeling contact in the mixed lubrication regime, considering surface topography, and implementing prediction models for ultrafast laser process parameter selection.

Alaitz ZABALA. She received her B.S. and Ph.D. degrees in mechanical engineering from Mondragon University, Spain, in 2010 and 2016, respectively. She is the coordinator of the Surface Technologies research group at Mondragon University since 2018. Her research interests include tribology, surface metrology, and surface functionalization applied to a wide range of industrial applications.